Radiation Physics and Chemistry ▮ (▮▮▮▮) ▮▮▮–▮▮▮

Contents lists available at SciVerse ScienceDirect

Radiation Physics and Chemistry

journal homepage: www.elsevier.com/locate/radphyschem

HMSPP nanocomposite and Brazilian bentonite properties after gamma radiation exposure

D.M. Fermino [a,*], D.F. Parra [a], W.L. Oliani [a], A.B. Lugao [a], F.R.V. Díaz [b]

[a] Nuclear and Energy Research Institute, IPEN-CNEN/SP, Av. Prof. Lineu Prestes 2242, Cidade Universitária, CEP 05508-000, São Paulo, SP, Brazil
[b] Department of Metallurgical and Materials Engineering, Polytechnic School, University of São Paulo, EPUSP, Av. Prof. Mello Moraes, 2463, Cidade Universitária, CEP 05508-000, São Paulo, SP, Brazil

ARTICLE INFO

Article history:
Received 1 January 2011
Accepted 1 January 2012

Keywords:
Modified PP
gamma irradiation
nanocomposite and bentonite

ABSTRACT

This work concerns the study of the mechanical and thermal behavior of the nanocomposite high melt strength polypropylene (HMSPP) (obtained at a dose of 12.5 kGy) and a bentonite clay Brazilian Paraiba (PB), which is known as "chocolate" and is used in concentrations of 5% and 10% by weight, in comparison to the American Cloisite 20A clay nanocomposites. An agent compatibilizer polypropylene-graft (PP-g-AM) was added at a 3% concentration, and the clay was dispersed using the melt intercalation technique using a twin-screw extruder. The specimens were prepared by the injection process. The mechanical behavior was evaluated by strength, flexural strength and impact tests. The thermal behavior was evaluated by the techniques of differential scanning calorimetry (DSC) and thermogravimetry (TGA). The morphology of the nanocomposites was studied with scanning electron microscopy (SEM), while the organophilic bentonite and nanocomposites were characterized by X-ray diffraction (XRD) and Fourier transform infrared spectroscopy (FTIR).

1. Introduction

In recent years, polymer layered silicate nanocomposites have attracted considerable attention both in fundamental research and industry and have been considered the new generation of composite materials (Touatii et al., 2007; Qin et al., 2005). The nanocomposites often exhibit excellent mechanical, thermal and gas barrier properties (Touatii et al., 2007; Bertini et al., 2006). It is projected that polymer/clay nanocomposites will play an increasingly important role as new materials in automotive, packaging, and aerospace applications (Touatii et al., 2007; Gu et al., 2004; Zhou et al., 2005; Sharma and Nayak, 2009).

The first major success with nanocomposites occurred when the Toyota Company produced nylon 6/clay composite with significant modulus and strength improvements (Abu-Zurayk et al., 2009; Usuki et al., 1993).

Polymer nanocomposites are polymers that have been reinforced with small quantities of nano-sized particles (nanofillers). These materials represent a radical alternative to conventionally filled polymers or blends. In conventional composites, the reinforcement is on the order of micrometers; polymer nanocomposites, however, are exemplified by discrete constituents on the order of nanometers (Ladhari et al., 2010).

Studies on the interaction between clay minerals and organic compounds have been conducted from the beginning of the 20th century, and the number of topics has increased. Research of the intercalation of organic molecules into the layer space of clay minerals began in the 1920s after the 1913 introduction of X-ray diffraction (Merinska et al., 2002; Paiva et al., 2008a).

An important class of nanofillers includes nanoclays that belong to the smectite group, such as montmorillonite. Montmorillonite belongs to the family of 2:1 layered silicates, and its structure has layers that are approximately 1 nm thick. Each layer consists of aluminum, magnesium oxide, and hydroxide (Ladhari et al., 2010).

Because of its excellent properties, which include a high cation exchange capacity, swelling behavior, adsorption and a large surface area, montmorillonite has been used extensively to prepare organoclays (Paiva et al., 2008a).

Clay is a natural hydrophilic material, which makes it difficult to exfoliate into a polymer matrix. To facilitate exfoliation, the surface treatment of silicate layers is necessary to render its surface more hydrophobic. Generally, this process can be performed by ion-exchange reactions with cationic surfactants, including primary, secondary, tertiary and quaternary alkylammonium cations (Lertwimolnun and Vergnes, 2005; Fornes et al., 2002; Le Pluart et al., 2002; Diagne et al., 2005; Dong and Bhattacharya, 2009, 2008; Wang et al., 2004a, 2004b; Perrin-Sarazin et al., 2005; Hasegawa et al., 1998).

The surface treatment increases the interlayer spacing and reduces the attractive forces between the clay layers that make

* Corresponding author.
E-mail addresses: dmfermino@usp.br (D.M. Fermino), dfparra@ipen.br.(D.F. Parra)

0969-806X/$ - see front matter © 2012 Elsevier Ltd. All rights reserved.
http://dx.doi.org/10.1016/j.radphyschem.2012.06.021

the intercalation of the polymer and/or the exfoliation and dispersion of the platelets possible (Touatii et al., 2007).

The clay layers can be either intercalated or exfoliated in the polymer matrix. In the intercalated nanocomposites, a monolayer of the extended polymer chain is inserted between the clay gallery to produce ordered stacks with fixed interlayer spacing. The exfoliated nanocomposites are formed when the individual clay layers are randomly dispersed in the polymer matrix (Usuki et al., 1993; Pavlidou and Papaspyrides, 2008).

Three methods are typically used to produce polymer nanocomposites: the intercalation of a suitable monomer followed by polymerization, the polymer intercalation from solution and the direct melt polymer intercalation. Intercalation of the polymer melts is the most attractive method because of its easy processibility, no solvent requirement and cost effectiveness (Diagne et al., 2005; Lertwimolnun and Vergnes, 2004).

However, for non-polar polymers such as polyolefins, the addition of compatibilizer-containing polar groups, such as maleic-anhydride-grafted poly(propylene) (PP-g-MA) copolymers, is necessary to enhance the diffusion of polymers into clay galleries (Diagne et al., 2005).

Moreover, the chemical reaction that occurs between maleic anhydride and hydroxyl groups at the edges of clay platelets is often responsible for peeling under shear forces (Diagne et al., 2005).

Processing parameters such as temperature, residence time and shear stress have significant effects on the structure of the resulting nanocomposites (Ray and Okamoto, 2003), which, in turn, influence the properties of the processed material. Nanocomposite properties strongly depend on the dispersion state of the clay; therefore, an evaluation of clay dispersion is important (Xie et al., 2010).

In addition, the relationship between compatibilizer chemistry and the processing conditions should be coupled because both might affect the exfoliation behavior. Thus, these two factors should be considered concurrently (Wang et al., 2004a,b).

A large variety of polymers have been used as matrices in the preparation of polymer/clay nanocomposites; polypropylene is commonly used because of an attractive combination of benefits, such as low cost, low weight, balance of properties and wide field applications (Ramos Filho et al., 2005; Han et al., 2006).

The use of traditional polypropylene resins in blown film processes has been prevented because of their poor melt strength and bubble instability. To overcome these deficiencies, it is necessary to improve the melt strength because it is apparent that opportunities exist for a high melt strength polypropylene resin in blown film (Oliani et al., 2010a).

The modification of a polymer with ionizing radiation can be performed before or after the polymer has been processed into formed parts. When formed polymer parts are modified by radiation, the desired reaction is crosslinking to enhance the physical properties of the parts (Cleveland et al., 2003; Cheng et al., 2010).

For radiation modification of polymer resins, various radiation-induced reactions, such as crosslinking, degradation, branching and grafting, add value to the polymer material prior to processing it into formed parts (Cheng et al., 2010).

Previous efforts to improve the melt strength of polypropylene resins focused on the introduction of long chain branching (Lugao et al., 2002, 2007) to increase the network entanglement level (Oliani et al., 2010a; Cheng et al., 2010; Ohnishi et al., 2005; Bhattacharya et al., 2009).

The grafting of long branches in this polymer improves its extensional viscosity in the molten state, which results in HMSPP. The increased melt strength and extensibility of the polymer melt is caused by the increased entanglement density of the macromolecules. This entanglement may be caused by branching in the chain of polydispersity of the material and in the cross-linking between chains (Oliani et al., 2010a,b; Chunxia et al., 2002).

The irradiation of polypropylene in an inert atmosphere causes a combination of chain scission and long-chain branching and results in a material with enhanced melt strength (Oliani et al., 2010b).

High-energy radiation, such as gamma and X-rays, e-beams and ion beams, have been widely used in the plastic and rubber industries because of their unique characteristics and advantages; therefore, there are a number of well-established industrial applications for radiation processing. The most relevant industrial applications are based on cross-linking technology, such as the wire and cable industry, packing films, foams, and radiation curing used on a large scale in surface finishing coatings, lacquers and inks (Otaguro et al., 2010).

The objective of this work is to obtain a polypropylene with high melt strength (HMSPP) through the process of gamma irradiation with a dose of 12.5 kGy. Using Brazilian clay treated in the laboratory, HMSPP will then produce nanocomposites that are comparable to American commercial clay.

2. Experimental

2.1. Materials and methods

2.1.1. Bentonite "chocolate" clay from the state of Paraiba treated in a laboratory

A sample of clay chocolate from the state of Paraiba (Brazil) was used. The sample was commercially and industrially transformed to form a sodium derivative, which was used, dried and sifted by passing it through an ABNT 200 mesh (0.075 mm opening). In a 2 L beaker, 960 g of distilled water and 40 g of bentonite clay were added. The addition was conducted using mechanical agitation concomitantly. Shortly thereafter, 64 g of quaternary ammonium salt (hexadecyltrimethylammonium chloride) was added, and agitation persisted for another 20 min to complete the salt dilution in the dispersion. This salt was used to transform the sodium clay into organophilic clay.

After 5 days, the clay settled at the bottom of the beaker; the dispersal (clay+water+salt) was removed, and the clay was washed. For the drying process, the clay was placed in an oven at a temperature of 60 °C for 52 h. The organoclay was ground in a mill with rotating blades to obtain powdered clay, which was sifted through an ABNT 150 sieve. A sample of Cloisite 20A organoclay (Southern Clay Products Inc.) was sifted in the same sieve through which the laboratory- treated clay was sieved; the organoclay was incorporated into the HMSPP.

The HMSPP used for the study was produced by the partnership between CBE Embrarad and IPEN and had a melt flow index of 2.2 g/10 min. The melt flow index of the starting material was 1.5 g/10 min.

The HMSPP samples were obtained by gamma irradiation with acetylene at 12.5 kGy of the total dose. The samples were irradiated in a ^{60}Co source at room temperature in an Embrarad/CBE cell at a rate of 10 kGy/h, and the dosimetry was performed with Harwell Red Perspex 4034.

After irradiation, the samples were heated for 60 min at 90 °C to eliminate the residual radicals (Oliani et al., 2010a). A 3% concentration (by weight) of the Polibond 3200 (Chemtura) coupling agent was used in all the samples except the pristine sample.

Please cite this article as: Fermino, D.M., et al., HMSPP nanocomposite and Brazilian bentonite properties after gamma radiation exposure. Radiat. Phys. Chem. (2012), http://dx.doi.org/10.1016/j.radphyschem.2012.06.021

2.1.2. Process of specimen extrusion and injection

The laboratory-treated bentonite "chocolate" clay and the bentonite Cloisite 20A clay with Irganox B215 FF (a blend of 0.2% of a sterically hindered phenol antioxidant and 0.4% of Irgafós, a thermal stabilizer) were manually mixed with Ciba Polibond 3200 (Chemtura company), a coupling agent that is also known as maleic anhydride (PP-g-MA), in a 3% concentration to improve the clay adhesion to the polymer matrix.

The Werner Pfleiderer twin screw extruder was used with a temperature range of 180 to 200 °C and a 600 rpm rotation to ensure the best homogeneity. A Battenfeld TM 750/210 injection was used to manufacture the specimens for flexural and impact tensile strength. The temperature of the nanocomposite injection was 190 °C, and the mold temperature was 60 °C.

2.1.3. Infrared spectroscopy (FTIR)

A ThermoNicolet spectrophotometer (model 380, FTIR with ATR accessory) was used to analyze the clay treatment, using the reflectance method to scan from 4000 cm^{-1} to 500 cm^{-1}.

2.1.4. X-ray diffraction (XRD)

The clay treatment and the nanocomposite specimens were analyzed with the Diffractometer Phillips X'Pert MPD, using Cu Kα radiation at the 1.5405 Å wavelength.

2.1.5. Mechanical tests

The tests were performed with an Instron Universal Testing Machine according to the ASTM D638 type 1 test standard for strength and the ASTM D790 standard for flexural tensile strength. The IZOD impact test was performed according to the ASTM D256 standard.

2.1.6. Thermal analysis

The melt and crystallization characteristics of the nanocomposites were studied with a Mettler Toledo DSC822^e differential scanning calorimeter (DSC). The specimens were subjected to temperatures of 25–280 °C at a heating rate of 10 °C min^{-1} in a nitrogen atmosphere. To study the nanocomposite mass loss, the Mettler Toledo SDTA851^e thermogravimetric analysis was used. The specimens were submitted to temperatures of 25 to 650 °C at a heating rate of 10 °C min^{-1} in an inert nitrogen atmosphere (N_2 flow 50 mL min^{-1}) and an oxygen atmosphere (O_2 flow 50 mL min^{-1}).

2.1.7. Gel and sol fractions

The gel fraction is the insoluble portion of a sample, which is determined after the solvent has been removed by vacuum drying and weighing. The gel fraction is determined by the ratio of the dry gel mass and the initial sample mass.

Analyses of the gel fraction were performed in a Soxhlet extraction apparatus with the PP sample placed in a stainless steel mesh (500 mesh) with xylene under boil to 138 °C for approximately 12 h with the solvent (Otaguro et al., 2010; Yoshiga et al., 2009; ASTM D 2765-01, 2006).

The sol fraction, the soluble portion of the samples, was obtained by settling in a beaker at room temperature (25 °C) with the total volatilization of xylene and the gradual deposition of a film of dry material in thin glass layers that are suitable for electron microscopy.

To measure the gel fraction, the initial PP concentration was approximately 0.3 g/100 cm^3.

Table 1
Identification specimens.

Specimen	Identification
HMSPP	HMSPP pristine
HMSPP AM	HMSPP with PP-g-MA
HMSPP B 5%	HMSPP with 5% in weight "chocolate" clay
HMSPP B 10%	HMSPP com 10% in weight "chocolate" clay
HMSPP C 5%	HMSPP com 5% in weight Cloisite 20A
HMSPP C 10%	HMSPP com 10% in weight Cloisite 20A

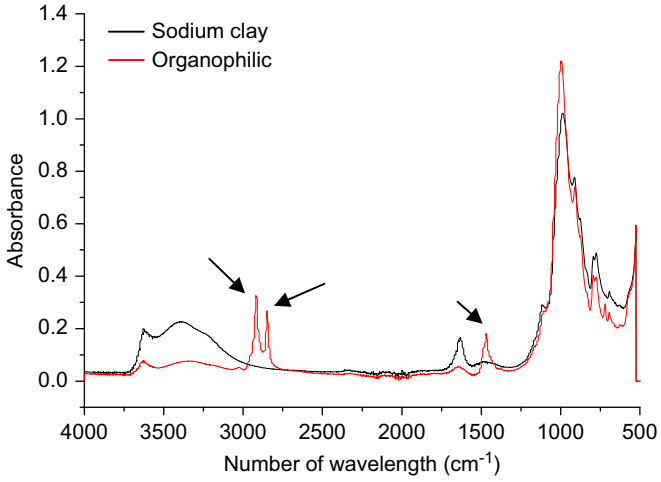

Fig. 1. FTIR spectrum "chocolate" clay.

2.1.8. Scanning electron microscopy (SEM)

Scanning electron microscopy was performed with an EDAX PHILIPS XL 30 instrument. The Balzers SCD 050 Sputter Coater was used to cover the samples with Au.

The nanocomposite identification is shown in Table 1.

3. Results and discussion

3.1. Infrared spectroscopy (FTIR)

Fig. 1 shows the spectra bentonite sodium clay and the organophilic clay.

Absorption bands were observed in the organoclay spectrum in the regions of 2917 cm^{-1} and 2849 cm^{-1}, which corresponded to the asymmetrical and symmetrical stretching of the CH bonds (CH_3 and CH_2; Paiva et al., 2008a,2008b).

The bands were also observed in the 1468 cm^{-1} region, which corresponded to angular deformations in the methylene group and stretching in the NH bond; this observation indicated that ammonium cations were intercalated between the montmorillonite galleries (Shishan et al., 2004).

3.2. X-ray diffraction (XRD)

Figs. 2 and 3 show the X-ray diffraction curves of the nanocomposites. Table 2 presents the basal spacing values that were obtained for the treated clay and the nanocomposites. The XRD test was used to evaluate the cation exchange efficiency. The quaternary ammonium salt increased the basal spacing of the laboratory-treated clay, demonstrating the effectiveness of the exchange.

The diffractograms data (as observed in Figs. 2 and 3 and Table 2) showed significant increases in the interplanar distances;

Please cite this article as: Fermino, D.M., et al., HMSPP nanocomposite and Brazilian bentonite properties after gamma radiation exposure. Radiat. Phys. Chem. (2012), http://dx.doi.org/10.1016/j.radphyschem.2012.06.021

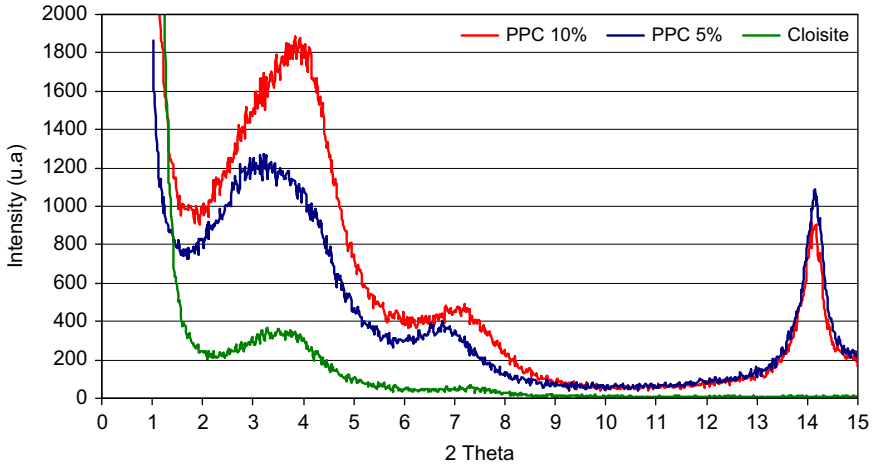

Fig. 2. XRD curves of nanocomposites with Cloisite clay.

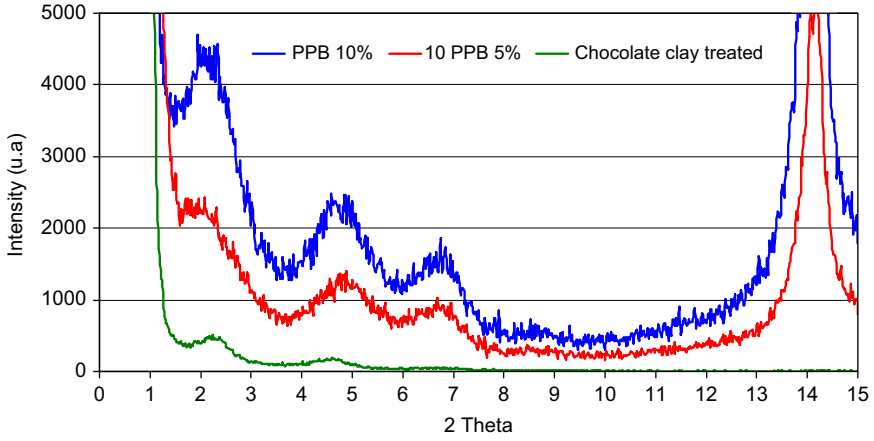

Fig. 3. XRD curves of nanocomposites with "chocolate" clay.

Table 2
Values of basal spacing obtained from the curves in Fig. 3.

	d_{001} (Å)
"Chocolate" clay (treated)	37.4
Cloisite 20A clay	24.4
HMSPPB 5%	44.7
HMSPPB 10%	43.9
HMSPPC 5%	28.0
HMSPPC 10%	22.6

therefore, there was intercalation of HMSPP in the clay. There were decreases in the intensity of the clay peaks in the nanocomposites compared to pristine clay (Figs. 3 and 4). This peak intensity reduction suggests that a major disorganization of lamellae is present in the clay nanocomposites. The nanocomposites have no completely exfoliated structures because the peak onset (001) indicates a minimum degree of intercalation.

3.3. Mechanical tests

The flexural strength values for the nanocomposite HMSPP at three points for maximum load (MPa) and Young's modulus 0–1% (MPa) are shown in Figs. 4 and 5, respectively.

In Fig. 5, the results indicate an increase in flexural strength with a maximum load of 9% for the nanocomposite HMSPPC 10% compared to HMSPP pristine. For the nanocomposite HMSPPB 10%, there was a 9% reduction compared to HMSPP and an 8% reduction over the HMSPPC 10% nanocomposite.

The addition of Cloisite 20A clay increased the Young's modulus measurement for the nanocomposites compared to the laboratory-treated chocolate clay nanocomposites. This increase occurs because the nanocomposites with Cloisite 20A clay provide better anchors than the laboratory-treated clay nanocomposites. There was an 8% increase in Young's modulus for the nanocomposite HMSPPC 10% compared to HMSPP pristine. The nanocomposite HMSPPB 10% decreased from 9% in the module in relation to HMSPP pristine.

This reduction might be due to the low interaction between the clay and polymer matrices because of the polarity difference. There was a 10% reduction in Young's modulus for HMSPP pristine and HMSPP AM.

Figs. 6 and 7 show the values of tensile strength (MPa) and elongation at break (MPa) that were obtained from tension tests for the nanocomposites with Cloisite 20A and the laboratory-treated bentonite "chocolate" clay.

The tensile strength values for the laboratory-treated clay nanocomposites were close to the values obtained for the Cloisite 20A clay nanocomposites.

The tensile strength values for the nanocomposites HMSPP with Cloisite 20A clay and HMSPP AM were identical. The tensile strength values of laboratory-treated nanocomposites with clay were somewhat lower compared to the nanocomposites with Cloisite 20A clay and the samples from HMSPP pristine and HMSPP AM.

Please cite this article as: Fermino, D.M., et al., HMSPP nanocomposite and Brazilian bentonite properties after gamma radiation exposure. Radiat. Phys. Chem. (2012), http://dx.doi.org/10.1016/j.radphyschem.2012.06.021

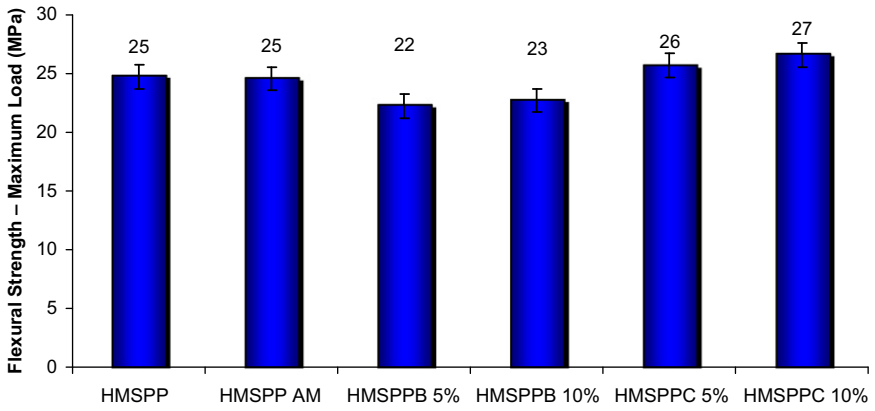

Fig. 4. Flexural strength – maximum load (MPa).

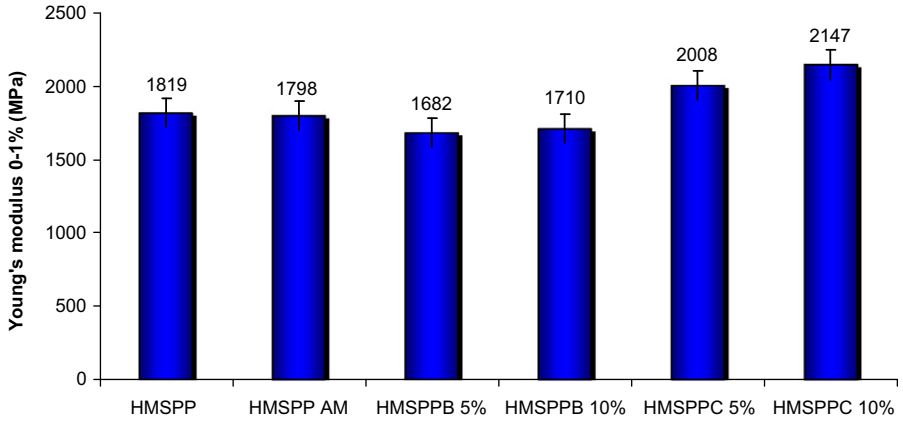

Fig. 5. Young's modulus 0–1% (MPa).

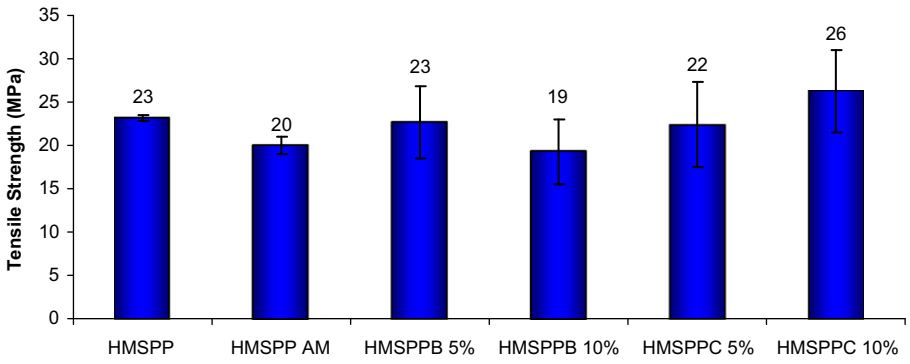

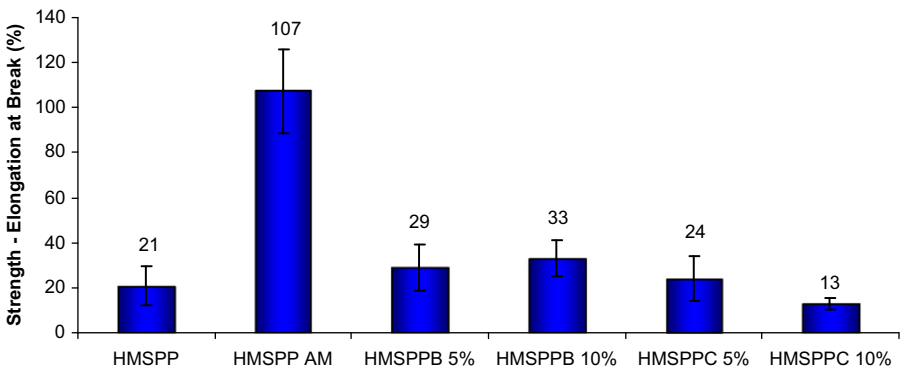

Fig. 7. Strength – elongation at Break (%).

Please cite this article as: Fermino, D.M., et al., HMSPP nanocomposite and Brazilian bentonite properties after gamma radiation exposure. Radiat. Phys. Chem. (2012), http://dx.doi.org/10.1016/j.radphyschem.2012.06.021

Fig. 6. Tensile strength (MPa).

The elongation at break for the HMSPP AM (AM=maleic anhydride) sample, showed the highest elongation compared to other samples. Only nanocomposite HMSPPC 10% obtained a lower elongation when compared with other samples; this lower elongation is because the smaller elongation strengthens the anchor between the clay and the polymer. The nanocomposites with Cloisite 20A demonstrated stronger anchoring in the polymer compared to the laboratory-treated clay.

Fig. 8 shows the IZOD impact values for the nanocomposites with Cloisite 20A clay and bentonite clay treated in the laboratory.

Regarding HMSPP pristine, the nanocomposite HMSPPB 10% showed the best impact test result. The other nanocomposites showed similar behavior. This improvement can be attributed to the absorption of impact energy by the clay and a reduction in the propagation of microcracks (Paiva et al., 2006).

In this test, HMSPP AM did not alter the impact properties in relation to HMSPP.

3.4. Thermal analysis

Figs. 9 and 10 show the DSC crystallization and melt curves, respectively, for the nanocomposites with Cloisite 20A clay and laboratory-treated bentonite. The crystallization peak temperature values are shown in Table 3, and Table 4 shows the nanocomposite temperature melt peaks.

Fig. 9 and Table 3 show the small insignificant changes in the crystallization temperature of HMSPP in relation to the nanocomposites with Cloisite and "chocolate" clay; the 3 °C change is not statistically significant.

Fig. 10 and Table 4 show slight changes in the melting temperatures of the nanocomposites of Cloisite clay and laboratory-treated clay. There was a temperature change of 2 °C, which is not statistically significant.

In general, the addition of nanoparticles in semi-crystalline polymers did not affect the crystallinity of the resulting nanocomposite materials; however, there may be some changes in particular nanocomposite systems. It has been proposed that these particles produce a much large number of nucleating sites and greatly reduce the size of the resulting spherulites (Chan et al., 2002).

Fig. 11 shows the TGA decomposition curves in an inert atmosphere (N_2) for the nanocomposites with Cloisite 20A clay and bentonite treated in the laboratory.

The thermal stability is the same for the nanocomposites Cloisite clay and laboratory-treated clay. For HMSPP pristine and HMSPP AM, decomposition (which was more pronounced in HMSPP AM) began at a lower temperature than in the nanocomposites.

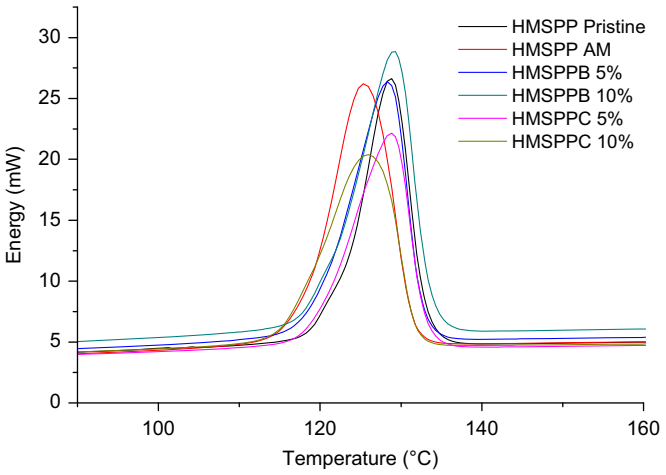

Fig. 9. Crystallization curves for the nanocomposites.

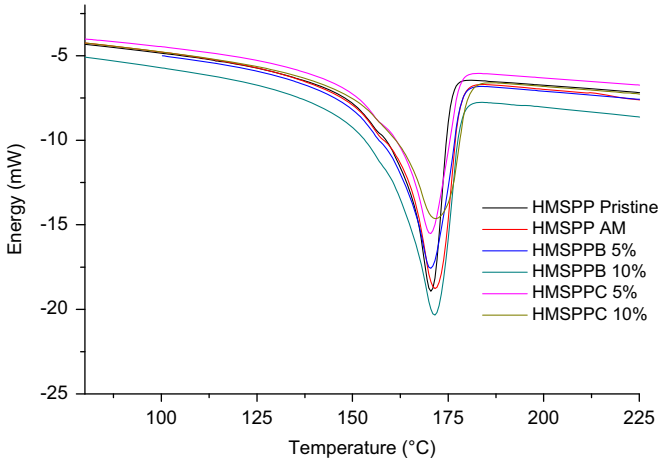

Fig. 10. Melt curves for the nanocomposites.

Table 3
Crystallization peak temperatures for the nanocomposites.

Peak (°C)	HMSPP pristine	HMSPP AM	HMSPPB 5%	HMSPPB 10%	HMSPPC 5%	HMSPPC 10%
	124	121	124	123	123	121

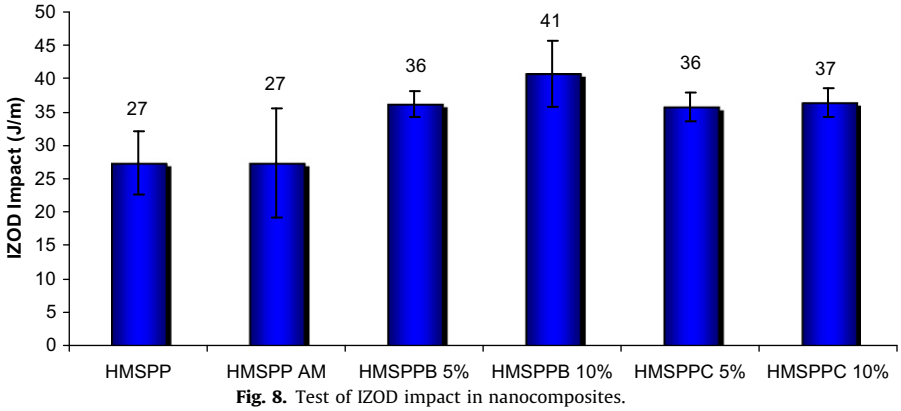

Fig. 8. Test of IZOD impact in nanocomposites.

Please cite this article as: Fermino, D.M., et al., HMSPP nanocomposite and Brazilian bentonite properties after gamma radiation exposure. Radiat. Phys. Chem. (2012), http://dx.doi.org/10.1016/j.radphyschem.2012.06.021

Table 4
Melt peak temperatures for the nanocomposites.

Peak (°C)	HMSPP pristine	HMSPP AM	HMSPPB 5%	HMSPPB 10%	HMSPPC 5%	HMSPPC 10%
	163	161	162	163	162	163

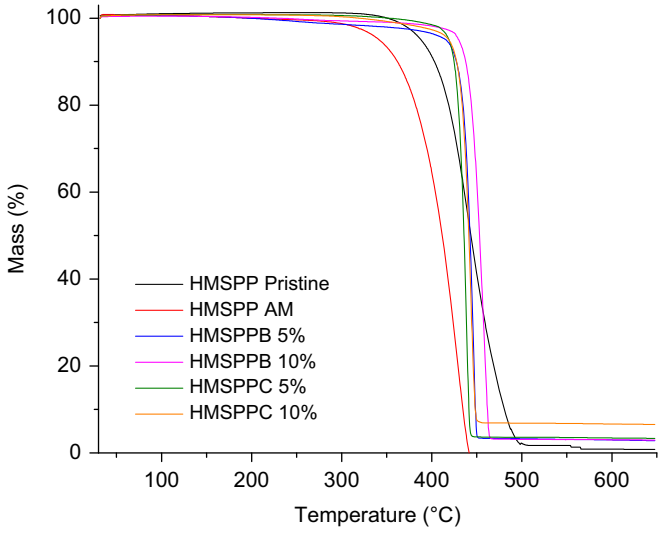

Fig. 11. TGA curves in a nitrogen atmosphere at a heating rate of 10 C min^{-1}.

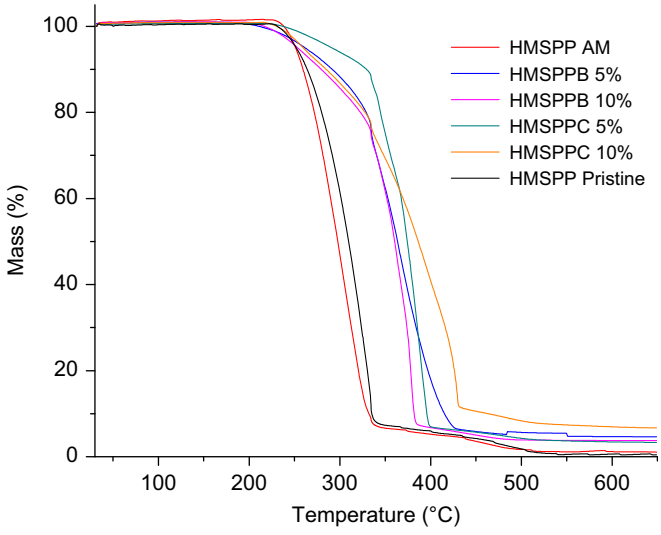

Fig. 12. TGA curves in an oxygen atmosphere at a heating rate of 10 °C min^{-1}.

In Fig. 12, the TGA decomposition curves are presented in a reactive atmosphere (O_2) for the nanocomposites with Cloisite 20A clay and laboratory-treated bentonite.

In an oxidizing atmosphere, the nanocomposites Cloisite 20A clay and laboratory-treated clay have similar profiles; HMSPP pristine and HMSPP AM are more sensitive to oxidation.

3.5. Gel fraction/sol fraction

Table 5 shows the results of the gel and sol fractions and the melt index in nanocomposites HMSPPB 10% and HMSPPC 10% and HMSPP pristine.

Table 5
Gel fraction/sol fraction results in nanocomposites HMSPPB 10% and HMSPPC 10% and HMSPP pristine.

Specimen	Gel fraction (%)
HMSPP pristine	0.5
HMSPPB 10%	0.5
HMSPPC 10%	0.6

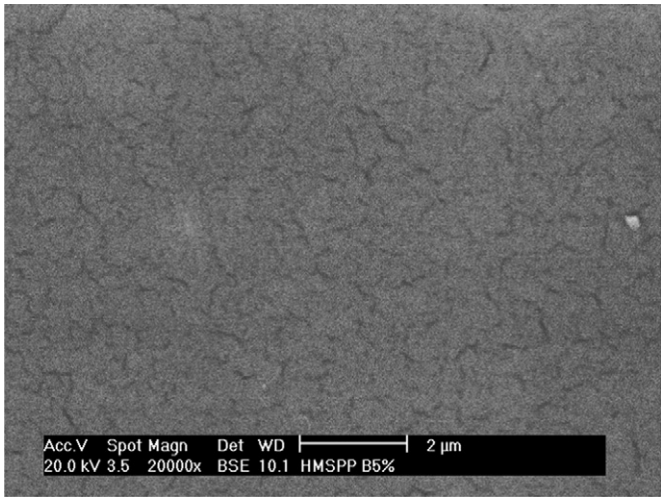

Fig. 13. HMSPPB 5% – 20,000x.

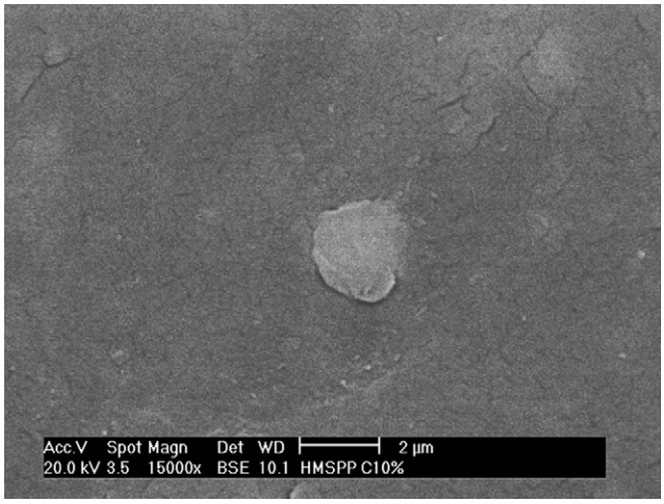

Fig. 14. HMSPPC 10% – 15,000x.

There was no change in the percentage of gel HMSPP pristine compared to the nanocomposites in HMSPPB 10% and HMSPPC 10% because all of the samples received the same dose of radiation.

3.6. Scanning electron microscopy (SEM)

Figs. 13 and 14 show two micrographs of nanocomposite HMSPPB 5% HMSPPC 10%, respectively. With SEM it was possible to observe the homogeneous distribution of the clay treated in the laboratory and the commercial clay added to the polymer matrix.

Please cite this article as: Fermino, D.M., et al., HMSPP nanocomposite and Brazilian bentonite properties after gamma radiation exposure. Radiat. Phys. Chem. (2012), http://dx.doi.org/10.1016/j.radphyschem.2012.06.021

Figs. 15–17 show the micrographs that were obtained with the samples volatilized on glass slides.

Figs. 18–20 show the micrographs that were obtained with the samples trapped in the steel screen used to determine the gel fraction

In the samples that were deposited on glass slides (Figs. 15–17), there are spherulites with diameters between 6 and 7 μm for all of the samples.

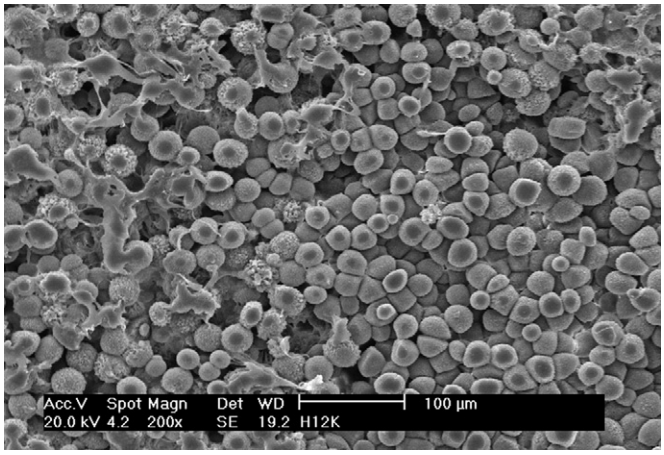

Fig. 15. SEM of gel HMSPP in glass lamina and substratum, HMSPP pristine, HMSPPB 10% and HMSPPC 10% in 100 μm.

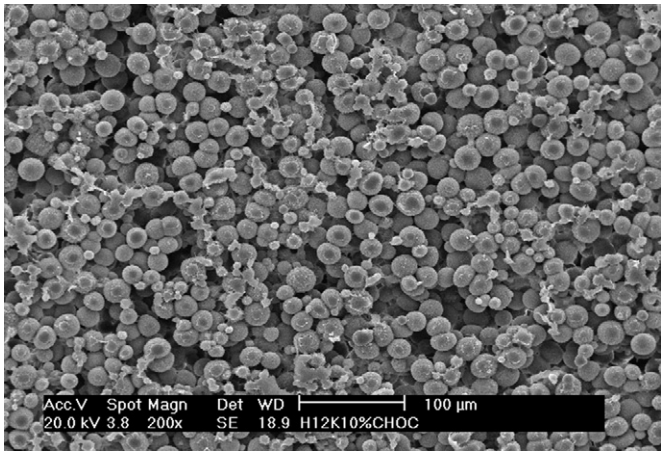

Fig. 16. SEM of gel HMSPP in glass lamina and substratum, HMSPP pristine, HMSPPB 10% and HMSPPC 10, in 100 μm.

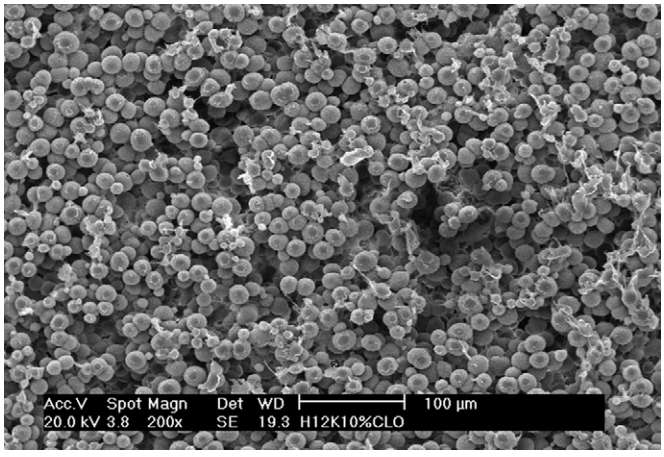

Fig. 17. SEM of gel HMSPP in glass lamina and substratum, HMSPP pristine, HMSPPB 10% and HMSPPC 10% in 100 μm.

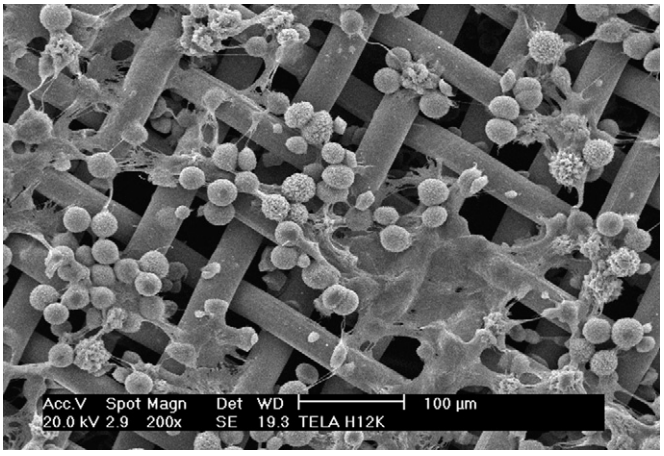

Fig. 18. SEM of gel HMSPP in steel screen, HMSPP pristine, HMSPPB 10% and HMSPPC 10, in 100 μm.

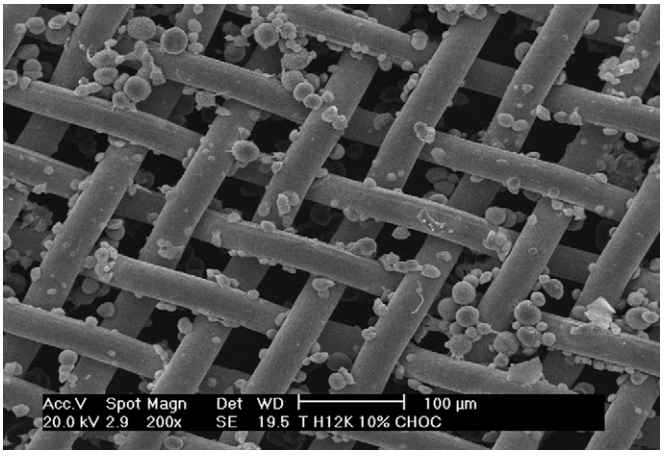

Fig. 19. SEM of gel HMSPP in steel screen, HMSPP pristine, HMSPPB 10% and HMSPPC 10, in 100 μm.

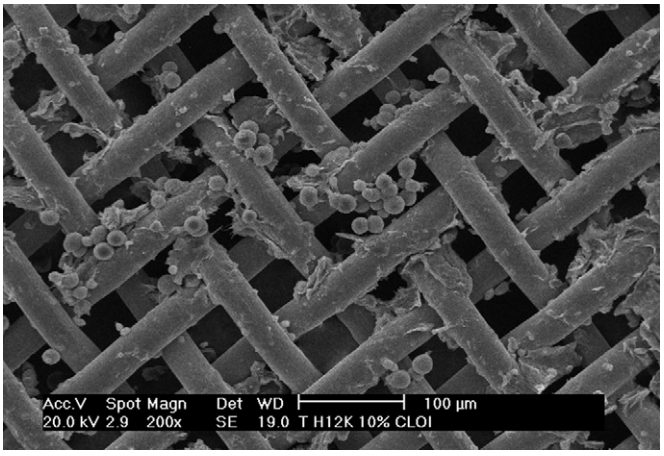

Fig. 20. SEM of gel HMSPP in steel screen, HMSPP pristine, HMSPPB 10% and HMSPPC 10, in 100 μm.

According to Matsuda et al. (1987), the gel diameter depends on the concentration used. They reported in this paper that a concentration of 1–5 g 100 cm^{-3}, where the gel was not formed and precipitated the polymer in solution, small spherulites with diameters of 10–30 μm were found.

Please cite this article as: Fermino, D.M., et al., HMSPP nanocomposite and Brazilian bentonite properties after gamma radiation exposure. Radiat. Phys. Chem. (2012), http://dx.doi.org/10.1016/j.radphyschem.2012.06.021

The clays used in the nanocomposites apparently influence the microgel formation, where numerous spherulites of minor size are observed.

4. Conclusion

The treatment of sodium clay in organophilic clay in the laboratory was successful (as tested by FTIR), and intercalated nanocomposites with clays did form (as demonstrated by the XRD test). A homogeneous load distribution was found, and there were some slight improvements in the mechanical properties of the nanocomposites with Cloisite 20A clay, which had better results compared to the nanocomposite clay treated in the laboratory.

In the thermal analysis, there were no significant changes in the crystallization and melting temperatures of the nanocomposites with the Cloisite 20A clay and the "chocolate" laboratory-treated clay compared with HSMPP pristine sample.

The clays influence the formation of HMSPP microgel, as demonstrated by the gel fraction tests and SEM (most likely through the nucleation mechanism).

Acknowledgments

The authors acknowledge The National Commission for the Nuclear Energy (CNEN) for financial support and the Quattor and Embrarad/CBE enterprises.

References

Abu-Zurayk, R., Harking-Jones, E., Mcnally, T., Menary, G., Martin, P., Armstrong, C., 2009. Biaxial deformation behavior and the mechanical properties of a polypropylene/clay nanocomposite 69, 1644–1652.

ASTM D 2765-01 (Reapproved 2006). Standard Test Methods for Determination of Gel Content and Swell Ratio of Crosslinked Ethylene Plastics.

Bertini, F., Canetti, M., Audisio, G.C., Falqui, L., 2006. Polym. Degrad. Stability 91, 600.

Bhattacharya, S., Gupta, R.K., Jollands, M., Bhattacharya, S.N., 2009. Foaming behavior of high-melt strength polypropylene/clay nanocomposites. Polym. Eng. Sci., 2070–2084.

Chan, C.M., Wu, J., Li, J., Cheung, Y., 2002. Polymer 43, 2981.

Cheng, S., Phillips, E.D., Parks, L., 2010. Processability improvement of polyolefins through radiation-induced branching. Radiat. Phys. Chem. 79, 329–334.

Chunxia, H., et al., 2002. Linear viscoelastic characterization of high-melt-strength polypropylenes over a broad range of frequencies. Available from: 〈http://www.rheofuture.de/papers2002/110902_ca_01.pdf〉 (accessed 18.09.10).

Cleveland, M., Parks, L., Cheng, S., 2003. Applications for processing of materials. Nucl. Instrum. Methods Phys. Res. Sect. B: Interact. Mater. Atoms 208, 66–73.

Diagne, M., Gueye, M., Vidal, L., Tidjaru, A., 2005. Polym. Degrad. Stability 89, 418.

Dong, Y.U., Bhattacharya, D., 2009. Dual role of maleated polypropylene in processing and material characterization of polypropylene/clay nanocomposites. Mater. Sci. Eng. A.

Dong, Y.U., Bhattacharya, D., 2008. Compos. Part A: Appl. Sci. Manuf 39, 1177–1191.

Fornes, T.D., Yoon, P.J., Hunter, D.L., Keskkula, H., Paul, D.R., 2002. Polymer 43, 5915–5993.

Gu, S.Y., Ren, J., Wang, Q.F., 2004. J. Appl. Polym. Sci. 91, 2427.

Han, D.H., Jang, J.H., Kim, H.Y., Kim, B.N., Shin, B.Y., 2006. Poly. Eng. Sci 46, 431.

Hasegawa, N., Kawasumi, M., Kato, M., Usuki, A., Okada, A., 1998. J. Polym. Sci 67, 87–92.

Ladhari, A., Daly, H.B., Belhadjsalah, H., Cole, K.C., Denault, J., 2010. Investigation of water absorption in clay-reinforced polypropylene nanocomposites. Polym. Degrad. Stabil. 95, 429–439.

Le Pluart, L., Duchet, J., Sauterau, H., Gerard, J.F., 2002. J. Adh 78, 645–662.

Lertwimolnun, W., Vergnes, B., 2005. Influence of Compatibilizer and Processing Conditions on the Dispersion of Nanoclay in a Polypropylene Matrix. Polymer 46, 3462–3471.

Lertwimolnun, W., Vergnes, B., 2004. Rheologie 5, 27.

Lugao, A., Noda, L., Cardoso, E., Hustzler, B., Tokumoto, S., Mendes, A., 2002. Temperature rising elution fractionation, infrared and rheology study on gamma irradiated HMSPP. Radiat. Phys. Chem. 63, 509–512.

Lugao, A., Artel, B., Yoshiga, A., Lima, L., Parra, D., Bueno, J., Liberman, S., Farrah, M., Tercariol, W., Otaguro, H., 2007. Production of high melt strength polypropylene by gamma irradiation. Radiat. Phys. Chem. 76, 1691–1695.

Matsuda, H., Inoue, T., Okabe, M., Ukaji, T., 1987. Study of polyolefin gel in organic solvents I. Structure of isotactic polypropylene gel in organic solvent. Polym. J. 19 (3), 323–329, Available from〈http://www.jstage.jst.go.jp/browse/polymj/_vols〉, (accessed 18.09.10).

Merinska, D., Malac, Z., Pospisil, M., Weiss, Z., Chrnielova, M., Capkova, P., Simonic, J., 2002. Polymer/clay nanocomposites on MMT/ODTA intercalates. Comp. Interf 9, 529–540.

Ohnishi, R., Fujimura, T., Tsunori, R., Sugita, Y., 2005. A new method for producing high melt strength poly(propylene) with reactive extrusion. Macromol. Mater. Eng. 290, 1227–1234.

Oliani, W.L., Lima, L.F.C.P., Parra, D.F., Dias, D.B., Lugao, A.B., 2010a. Study of the morphology, thermal and mechanical properties of irradiated isotactic polypropylene films. Radiat. Phys. Chem. 79, 325–328.

Oliani, W.L., Parra, D.F., Lugao, A.B., 2010b. UV stability of HMSPP (high melt strength polypropylene) obtained by radiation process. Radiat. Phys. Chem. 79, 383–387.

Otaguro, H., Lima, L.F.C.P., Parra, D.F., Lugao, A.B., Chinelatto, M.A., Canevarolo, S.V., 2010. High-energy radiation forming chain scission and branching in polypropylene. Radiat. Phys. Chem. 79, 318–324.

Paiva, L.B., Morales, A.R., Diaz, F.R.V., 2008a. Organoclays: properties, preparation and applications. Appl. Clay Sci. 42, 8–24.

Paiva, L.B., Morales, A.R., Diaz, F.R.V., 2008b. Argilas organofílicas: características, metodologias de preparação, compostos de intercalação e técnicas de caracterização. Cerâmica 54, 213–226.

Pavlidou, S., Papaspyrides, C.D., 2008. A review on polymer-layered silicate nanocomposites. Prog. Polym. Sci. 33, 1119–1198.

Paiva, L.B., Morales, A.R., Guimarães, T.R., 2006. Propriedades mecânicas de nanocompósitos de polipropileno e montmorilonita organofílica. Polím.: Ciência Tecnol 16 (2), 136–140.

Perrin-Sarazin, F., Ton-That, M.T., Bureau, M.N., Denault, J., 2005. Polymer 46, 11624–11634.

Qin, H., Zhang, S., Liu, H., Xie, S., Yang, M., Shen, D., 2005. Polymer 46, 3149.

Ramos Filho, F.G., Melo, T.J.A., Rabello, M.S., Silva, S.M.L., 2005. Polym. Degrad. Stabil. 89, 383.

Ray, S.S., Okamoto, M., 2003. Polymer/layered silicate nanocomposites: a review from preparation to processing. Prog. Polym. Sci. 28, 1539.

Sharma, S.K., Nayak, S.K., 2009. Surface modified clay/polypropylene (PP) nanocomposites: effect on physico–mechanical, thermal and morphological properties. Polym. Degrad. Stabil. 94, 132–138.

Shishan, W., Dingjun, J., Xiaodong, O., Fen, W., Jian, S., 2004. Polym. Eng. Sci. 44, 2070.

Touatii, N., Kaci, M., Ahouari, H., Bruzaud, S., Grohens, Y., 2007. The effect of gamma irradiation on the structure and properties of poly(propylene)/clay nanocomposites. Macromol. Mater. Eng. 292, 1271–1279.

Usuki, A., Kojima, Y., Kawasumi, M., Okada, A., Fukushima, Y., Kurauchi, T., et al., 1993. Synthesis of nylon 6 clay hybrid. J. Mater. Res. 8, 1179–1184.

Wang, Y., Chen, F.B., Li, Y.C., Wu, K.C., 2004a. Compos. Part B: Eng 35, 111–124.

Wang, Y., Chen, F.B., Li, Y.C., Wu, K.C., 2004b. Melt processing of polypropylene/clay nanocomposites modified with maleated polypropylene compatibilizers. Compos.: Part B 35, 111–124.

Xie, S., Harkin-Jones, E., Shen, Yucai, S., Hornsby, P., Mcafee, M., Mcnally, T., Patel, R., Benkreira, H., Coates, P., 2010. Quantitative characterization of clay dispersion in polypropylene–clay nanocomposites by combined transmission electron microscopy and optical microscopy. Mater. Lett. 64, 185–188.

Yoshiga, A., Otaguro, H., Parra, D.F., Lima, L.F.C.P, Lugao, A.B., 2009. Controlled degradation and crosslinking of polypropylene induced by gamma radiation and acetylene. Polym. Bull., 63, 397-409, Available from〈http://www.periodicos.capes.gov.br〉, (accessed 18.09.10).

Zhou, Y., Rangari, V., Mahfuz, H., Jeelani, S., Mallick, P.K., 2005. Mater. Sci. Eng 402, 109.

Please cite this article as: Fermino, D.M., et al., HMSPP nanocomposite and Brazilian bentonite properties after gamma radiation exposure. Radiat. Phys. Chem. (2012), http://dx.doi.org/10.1016/j.radphyschem.2012.06.021